Understanding and modeling the liquid uptake in porous compacted powder preparations

Esteban, Jesus; Moxon, Thomas; Simons, Tom; Bakalis, Serafeim; Fryer, Peter

DOI:
10.1021/acs.langmuir.7b01334

Document Version
Peer reviewed version

Citation for published version (Harvard):
Esteban, J, Moxon, T, Simons, T, Bakalis, S & Fryer, P 2017, 'Understanding and modeling the liquid uptake in porous compacted powder preparations', *Langmuir*, vol. 33, no. 28, pp. 7015–7027. https://doi.org/10.1021/acs.langmuir.7b01334

Understanding and modeling the liquid uptake in porous compacted powder preparations

Journal:	*Langmuir*
Manuscript ID	la-2017-01334t.R2
Manuscript Type:	Article
Date Submitted by the Author:	n/a
Complete List of Authors:	Esteban, Jesus; University of Birmingham, School of Chemical Engineering Moxon, Thomas; university of Birmingham, School of Chemical Engineering Simons, Tom; University of Birmingham, Chemical Engineering Bakalis, Serafim; University of Birmingham, Chemical Engineering Fryer, Peter; University of Birmingham, Formulation Engineering

Understanding and modeling the liquid uptake in porous compacted powder preparations

Jesús Esteban*, Thomas E. Moxon, Tom A.H. Simons, Serafim Bakalis, Peter J. Fryer
School of Chemical Engineering.University of Birmingham. Edgbaston. Birmingham B15 2TT, United Kingdom.
*Corresponding author: J.Esteban@bham.ac.uk / jesus_esteban@quim.ucm.es (Phone number: +44 (0) 121 414 5081)

Abstract

Porous solid materials commonly undergo coating processes during their manufacture, where liquids are put in contact with solids for different purposes. The study of liquid penetration in porous substrates is a process of high relevance in activities in several industries. In particular, powder detergents are subject to coating with surfactants that will boost their performance, although this may affect the flowability and even cause caking of the particulate material, which can be detrimental to consumer acceptance.
Here we present a methodology to make compacted preparations of powders relevant to detergent making and evaluate the internal structure of such porous substrates by means of X-ray micro-computed tomography.
Liquid penetration into the preparation and total mass uptake of fluid were monitored by a gravimetric technique based on a modified Wilhelmy plate method consisting of consecutive cycles. Taking into account the geometry of the system, two models were proposed to describe the liquid uptake, based on the process being driven by mass (Model 1) or pressure (Model 2) gradients. Comparison between both from a statistical and physical point of view led to the conclusion that the latter was more appropriate to describe the process, retrieving values of the permeability of the solid between 0.03 and 0.95×10^{-12} m^2. Finally, with the parameters retrieved from Model 2, the force balance observed throughout the experiment was simulated satisfactorily.

Keywords: powder compaction, porous media, dynamic wetting, liquid uptake, Darcy's law.

Introduction

Penetration and imbibition of liquids into porous media occurs in many events in nature and industry alike. In the former, the absorption of water by seeds or dry wood and irrigation are paradigmatic examples, whereas in the latter liquid penetration is a phenomenon of relevance in applications and processes like multiphasic catalytic reactions, ink-jet printing, flotation in mining, fabric dying or coating of materials [1].

Coating is a process of particular interest to activities like detergent processing and other powdered products of the fast moving consumer goods industries. Attention must be paid to fluid penetration into the porous substrate, for the effectiveness of the process and the subsequent final quality of the product is directly related to the extent of such penetration. For instance, the appearance of particles and their performance in phenomena like dissolution are directly linked to fluid penetration.

Tablets made from powders under different conditions have been used in many studies for the evaluation of phenomena like moisture transport [2], mechanical strength and dissolution [3], disintegration [4] or drug release [5]. Preparation of tablets of controlled porosity by compaction of powders using compaction simulators or similar devices has been previously reported in literature [6, 7].

Different authors have employed a number of techniques for the analysis of the porosity and internal structure of porous bodies. The common denominator of these methods is their non-invasive and non-destructive nature. For instance, the internal porosity of formulations made of microcrystalline cellulose and croscarmellose sodium has been analysed using terahertz spectrometry [6, 7]. X-ray microscopy has been used for the characterization of the porosity and tortuosity of membranes [8]. In particular, X-ray microcomputed tomography (μ-CT) is a very effective method that allows the visualization of the internal structure of solids. This technique has been put to use in multiple applications like the analysis of biomaterials, artistic works and food samples [9-11]. Of particular interest to the study herein dealt with, μ-CT has proven effective in the evaluation of the solid fraction of pharmaceutical tablets made under different environmental conditions [2].

Powder wettability has also been studied by a range of approaches [12]. These include sessile drop studies evaluating the penetration of droplets of a liquid into porous powder beds [13-16] or liquid rise on columns through capillary rise [17-20] . Another technique is the Wilhelmy plate, which has been widely used to determine mass uptake,

swelling, stability and contact angles of materials like wood [21-25], pharmaceutical powders [26-28] or polymeric materials [29]. For Wilhelmy plate derived experiments, compaction of powders has been a common method for the preparation of samples [17].

A number of authors have investigated how to model different types of processes related to wetting of porous substrates. Wetting through capillary rise has been explained traditionally by the Lucas-Washburn equation [30], which has been applied to the spontaneous wetting of different porous media [31-33]. Cai et al. [34] recently derived a full analytical expression to describe the spontaneous imbibition of a wetting liquid into fractal porous media. In addition, Ding et al. [35, 36] also developed the analytical modeling of liquid penetration in slot die coating processes, including the development of a CFD model.

The industry needs experimental methodologies and models to predict the mass uptake in coating experiments. The purpose of this work is to study the coating of particles, for which an approach based on tableting such particles was followed to study the mentioned phenomenon as a function of the properties of both the liquid and the solid substrate. Given the precedent work on the wetting of porous solids, the major goals of this study are: (a) to present a methodology to prepare tablets of controlled porosity from compaction of powdered material and (b) to identify the driving mechanisms to study and model the dynamic wetting and liquid uptake of the tablet upon contact and withdrawal from a pool of non-dissolving liquid.

Experimental Section

Materials

The powder materials employed in this work were supplied by the Procter & Gamble Company. They consist of porous spray-dried granules with a size distribution of d_{10}=357.11 μm, d_{50}= 463.33 μm and d_{90}=580.29μm as measured by a QicPic Particle size analyser (Sympatec GmbH). Their composition is relevant to the manufacture of powder detergents and features varying amounts of different sodium salts, linear alkylbenzene sulfonate as surfactant, polymer binder and optical brightener (Tinopal) to render the tablet visible under a fluorescent microscope. Prior to compaction, any remaining moisture within their composition was removed by drying using a MA160 Sartorius thermal balance.

As for the liquid materials, oleic acid (98% purity, Sigma Aldrich) and Neodol 45-7 (Shell Chemicals) were utilized for the dipping experiments. The latter chemical is a commercial mixture typically used as a non-ionic surfactant in industrial practice that consists in fatty alcohols of chain lengths C14-C15 and an average molar ratio of 7 to 1 of ethylene oxide to fatty alcohol. These were chosen due to their surfactant nature and the fact that they did not dissolve the powders.

Preparation of porous substrate samples

Porous preparations of approximately 0.25 g were assembled by compaction of powders into circular tablets using a punch and die of 13 mm of diameter within an Instron Microtester model 5848 (Norwood, MA, USA) was used. The Microtester is equipped with a load cell that could apply forming forces of up to 2000 N so that varying porosities of the preparations could be achieved. After preparation, samples were kept in a desiccator to prevent any undesired moisture uptake from the atmosphere. Final tablet size was of 13 ± 0.03 mm with thicknesses varying between 1.25 and 2.30 mm depending on the force applied to form the tablet.

Analysis of the internal structure of the substrates

The internal structure of the compacted preparations was analysed by means of X-ray microcomputed tomography (μ-CT) using a Skyscan 1172 device (Bruker, Brussels, Belgium). Scans were acquired with a camera with a resolution of 6.76 μm per pixel using a round scanning trajectory (0.400 degrees per step) and no filter. To achieve an appropriate resolution, the X-ray source was set at a voltage of 50 kV and a current of 90 mA and an exposure time of the camera of 350 ms. Images were reconstructed using the SkyScan NRecon package applying ring artefacts reduction and beam hardening correction to reduce noise in the images.

Using the reconstructed set of images, characterisation of the internal structure of the substrates was conducted with the CTAn (v.1.15.4.0) software. The procedure consisted in defining a volume of interest to which a series of image analysis operations would be applied: global thresholding for binarisation, removal of speckles constituting noise pixels, shrink-wrap of the volume of interest to fit to the physical borders of the sample and finally 3D analysis to determine the structural parameters of the solid.

Measurement of liquid uptake

After analysis of the internal structure, the porous substrates were analysed for liquid uptake. Tablets were glued to a small plastic toothpick and then mounted on a Krüss tensiometer model K-100 (Hamburg, Germany) in lieu of a conventional Wilhelmy plate. The solid was dipped into the pool of liquid to a depth of 10 mm to ensure that no liquid would be in contact with the top part of the tablet.

Figure 1(a) depicts the rest of the experimental setup, which has a glass vessel placed in a jacketed holder connected to a temperature-controlled bath (Tecam TE-7 Tempette, Italy). To perform the dynamic wetting experiments the liquid level was raised and lowered in alternate cycles using a Pump11 Elite syringe pump (Harvard Apparatus, United States) controlling the infusion and withdrawal rate to adjust to the desired immersion or emersion speed in a similar way to the experiments devised by Moghaddam et al. for the measurement of water uptake of wood [21-24]. Figure 1(b) shows a sketch of the immersion/emersion of the tablet into the liquid medium. The total mass uptake after each cycle can be determined from the force measurement after removal of the tablet from the pool of liquid. Thickness of the tablets was measured for swelling with an electronic micrometer dismounting the sample from the tensiometer at the end of each cycle.

Preparation of samples and visualization under fluorescent microscope

As stated in Section 2.1, the formulation of the powders contained an optical brightener so that the tablet would become visible under fluorescent light. After the dipping experiments, the tablets were mounted on a 25:3 v/v mixture of Epofix ® Resin and Epofix ® Hardener and allowed to dry for 24 hours. This protocol ensured proper fixing and made it easy to obtain a clean cross section in the direction of the flow of the liquid by scraping the resin with graining paper.

The samples were then visualized under a Z16 AP0A microscope (Leica Microsystems, Germany) equipped with a pE-100 fluorescent excitation light source (CoolLED, UK) at 400 nm. The images were acquired using a digital camera mounted with a DD63NLC adapter (Diagnostic Instruments, USA). Observation of the emission profiles was done using the open source software ImageJ 1.49v (National Institute of Health, USA).

Measurement of the properties of the liquids

In addition to the multicycle dynamic wetting of the porous solids, the tensiometer was used to determine the surface tension and the density (measurements based on the Archimedes principle) of the liquids used for testing. Viscosities were measured using an AR-G2 rotational rheometer (TA Instruments, Ltd., Delaware, USA) fitted with cone and plate geometry with a cone angle of 2° and a diameter of 60 mm. Further details may be found in previous work [37].

Results

Internal characterization of tablets

The powder granules loaded for compaction in the particle microtester were subject to normal force loads ranging from 100 to 2000 N. When applied to the circular geometry of the punch and die, such loads correspond to 0.75 MPa and 15 MPa in accordance with the surface area of the tablet (ϕ= 13 mm). Below a load of 0.75 MPa, preparations were too brittle to be further manipulated and analysed by μ-CT.

Figures 2(a) and 2(b) show three-dimensional reconstruction of scanned tablets of high and low porosities pressed at 0.75 MPa and 15 MPa, respectively. First, it can be seen that the thickness of the tablets varies taking into account that each mark of the box wrapping the reconstructed table represents a length of 1 mm. This obviously affects the degree of packing of the granules within the tablet structure, which will hold an effect on the overall porosity. A quarter of the tablet was cut from the reconstruction to show further how the internal packing differs in both cases.

Figure 3 shows the overall porosity of the tablets as a function of the pressure applied to make them, where the error bars represent the variance of the observed porosities in quintuplicate experiments. In general, decreasing porosity results from the application of an increasing pressure. It can be seen that at low forming pressures the variation of porosity is quite evident, whilst at 11.3 MPa and above such variation is less significant.

This behaviour can be well described using the derivation of the Kawakita equation [38] as described in literature, which leads to equation 1 [39]:

$$\ln\frac{1}{\phi} = \ln\frac{1}{\phi_0} + \ln\left(1 + b\left(1-\phi_0\right)\right)P \qquad \text{[eq.1]}$$

where ϕ is the observed porosity of the tablet, ϕ_0 is the initial porosity of the powder (0.5664) and b is the fitting parameter of the Kawakita equation. From the fitting, the

intercept was 0.5906 and the parameter b acquired a value of 0.1862, with a R^2 value of 0.9169.

Whilst the compressibility of powders and the resulting porosity from compression depends on their chemical composition, the results obtained in this work are qualitatively in line with those observed in literature. For example, the overall porosity of tablets made of sodium dihydrate dichloroisocyanurate, a component relevant in the formulation of industrial disinfectant tablets, ranged from approximately 30% when compaction took place at 30 MPa to 10% at 300 MPa [40]. For coal samples subjected to different pressures, a decrease in porosity was observed as pressure increased. In this case, the overall porosity dropped approximately 1 to 2 % for different samples of circa 10% porosity for pressures ranging from 3 to 15 MPa following a linear decay[41].

3D analysis obtained from μ-CT scans also allows the open and closed porosity to be obtained. These can be defined as the relative amount of pores present in the structure that are connected or not connected to the outer surface of the sample [37, 38]. In addition, this tool allows calculating the pore size distribution of the tablet [41-43], which will help to calculate an effective pore size following equation 2 [44]:

$$d_p = \sum w_i \cdot d_i \qquad \text{[eq.2]}$$

where w_i is the relative amount of pores of a size d_i. Table 1 presents the data obtained for the tablets of each experiment and the conditions at which experiments were performed.

Description of the experiment

The events taking place in the experiments are shown in Figure 4, which depicts the evolution of one cycle of the dynamic wetting test using the tensiometer:

(i) Before any contact with the liquid, the force recorded by the instrument remains at zero after taring the balance (A).

(ii) Then, upon contact of the sample with the liquid, an increase in force is observed caused by the surface tension (B); this point marks the starting point of the experiment (t=0 s).

(iii) Thereafter, as the tablet is immersed into the fluid the net force observed declines due to buoyancy effects until it reaches a minimum after 60 s (C),

which corresponds to the maximum depth of the body within the liquid attained (10 mm) and hence the maximum buoyancy.

(iv) Beyond this point, the liquid level decreases leaving less and less of the tablet immersed, thus recording a higher net force acquiring positive values again, until a point (D), where a maximum is reached at time 120 s.

(v) Then, a slight decline is noted while a liquid meniscus is still present followed by an abrupt drop, which corresponds to its breakage (E). The force recorded after the complete withdrawal of the porous substrate from the liquid can be related to the weight gained by liquid uptake.

Figure 5 shows images taken under a fluorescent microscope for cross sections of the tablets cut halfway through their thickness. The pictures correspond to two extreme cases: (a) a tablet of high porosity (43.55%) after six dipping cycles and (b) a tablet of low porosity (18.99%) after only one cycle. On their right-hand side are the intensity profiles of the lines crossing the diameter of the tablets both horizontally (black curve) and vertically (red curve). Such profiles show the light intensity of the image as a grey scale ranging from 0 (black) to 255 (white), where the brightest values correspond to the fluorescence emitted by the optical brightener within the tablet. As the tablet contacts the liquid, the signal attenuates and the parts with a higher exposure to the liquid acquire darker values on the scale.

For both tablets the trends of the horizontal profiles show almost symmetrical profiles reaching higher values towards the central part of the tablet. This is clear evidence that the liquid flows into the tablet from the outer surface to the interior of the tablet. There the fluorescence intensity reaches its highest value, as it remains more inaccessible to the liquid than the edges. In the case of Figure 5(a), the profile line is smoother than in Figure 5(b), which accounts for the fact that after 6 cycles, the liquid has flowed more homogeneously into the internal structure of the tablet. For the less porous tablet with less contact with the liquid, a more pronounced profile can be seen, as observed for Figure 5(b), where at approximately 2.5 mm from the edges maximum values of the intensity are attained.

As for the trends of the vertical profile lines, a decrease can be observed from the top to the bottom. First, down to about 2.5 to 3 mm, the intensity practically remains at maximum values, as the top 3 mm of the tablet were not in contact with the liquid at all. Then, from 3 mm to the bottom there is a general declining trend, which is caused by the bottom part of the substrate remaining dipped in the liquid reservoir for a longer

period of time. Again, for the case (a), the profile follows a smoother pattern than in (b) due to more liquid being present inside the tablet.

Modelling the liquid uptake process

Tablet swelling

During the experiments the tablets were observed to undergo some swelling. For modelling purposes, it will be assumed that this swelling only occurs in the direction perpendicular to the radial plane; i.e., there is an increase in the tablet thickness, but no change in the diameter of the tablet. Also, it will be considered that the change in thickness is uniform over the whole tablet. An empirical power law model is proposed to describe observed swelling as a function of the fractional mass increase observed, as depicted in Figure 6. The fitting obtained is shown in equation 3, which has a R^2 value of 0.93:

$$\Delta\delta = 5.17 \cdot \Delta m^{0.47} \qquad \text{[eq.3]}$$

where Δm is defined as the mass increment due to uptake with respect to the initial mass ($\Delta m = \frac{m-m_0}{m_0}$). The thickness of the tablets was manually measured using a micrometer, contrary to the perimeter model used in other works that uses a non-swelling liquid like octane [21, 23]. The latter method could not be implemented here given the composition of the samples, which were both soluble in octane due to the presence of the polymer and in water owing to the sodium salts, hence disrupting the structure of the compacted powder preparation.

Geometry of the system

One feature of the experimental set up is the varying contact area throughout time between the liquid and different points on the tablet. This is displayed in Figure 7, where we can define a variable *h(t)*, which is the height of liquid relative to the bottom of the tablet at a given time, *t*. The tablet can be broken up into $\frac{2R}{dx}$ bands, which are at a distance *x* above the base of the tablet.

The dipping speed is constant throughout each test and once the maximum height of liquid on the tablet is reached (h_{max}), the direction of the liquid flow is reversed and, subsequently, the liquid is removed at the same speed without any pause at the maximum point.

As such, the variation of the height with time over the domain $t \in [0, t_{max}]$ can be described with a triangular wave function:

$$h(t) = \frac{h_{\max}}{\pi} \sin^{-1}\left(\sin\left(\frac{2\pi}{t_{\max}}\left(t - 0.25t_{\max}\right)\right)\right) + \frac{h_{\max}}{2} \quad \text{[eq.4]}$$

The maximum time can be defined from the dipping speed:

$$t_{\max} = \frac{2h_{\max}}{u} \quad \text{[eq.5]}$$

in which u is the immersion speed of the tablet into the liquid.

From the description of the liquid height and the definition of the area of a circular segment, equation 6 is obtained:

$$A_{seg} = \frac{R^2}{2}\left(\alpha - \sin\alpha\right) \quad \text{[eq.6]}$$

where α is the angle that the circular sector forms from the center with respect to the height of the liquid front as depicted in Figure 7, which corresponds to:

$$\alpha = 2\cos^{-1}\left(1 - \frac{x}{R}\right) \quad \text{[eq.7]}$$

Thus, we can produce equations to define how the contact area (A) and submerged volume (V) vary with time both for the total area and volume (equations 8(a) and 9(a)) and the corresponding differential elements (equations 8(b) and 9(b)):

$$A(t) = \int_0^{h(t)} \frac{2\delta + 2R\left(1 - \cos\left(2\cos^{-1}\left(1 - \frac{x}{R}\right)\right)\right)}{\sqrt{1 - \left(1 - \frac{x}{R}\right)^2}} dx \quad \text{[eq.8a]}$$

$$A|_x = \int_{x-dx}^{x} \frac{2\delta + 2R\left(1 - \cos\left(2\cos^{-1}\left(1 - \frac{x}{R}\right)\right)\right)}{\sqrt{1 - \left(1 - \frac{x}{R}\right)^2}} dx \quad \text{[eq.8b]}$$

$$V(t) = \int_0^{h(t)} R.\delta.\left(\frac{1 - \cos\left(2\cos^{-1}\left(1 - \frac{x}{R}\right)\right)}{\sqrt{1 - \left(1 - \frac{x}{R}\right)^2}}\right) dx \quad \text{[eq.9a]}$$

$$V|_x = \int_{x-dx}^{x} R.\delta.\left(\frac{1 - \cos\left(2\cos^{-1}\left(1 - \frac{x}{R}\right)\right)}{\sqrt{1 - \left(1 - \frac{x}{R}\right)^2}}\right) dx \quad \text{[eq.9b]}$$

where R is the tablet radius, and δ is the tablet thickness, which is a function of the mass at time t as described by equation 3.

Saturation concentration

After a certain mass of liquid is adsorbed, the tablet will become saturated and there will be no further increase in the tablet weight, as can be seen in the plots of mass uptake against cycle (Figure 8). It can be observed that the majority of the liquid uptake occurs after the first contact cycle and then a plateau is reached, usually after the third cycle.

We can therefore define a saturation concentration (C_{sat}), which will depend on the liquid and solid properties, and the parameter will be calculated from the experimental mass absorbed after the final cycle (m_n), divided by the available volume- the tablet volume multiplied by the open porosity ϕ_{open}:

$$C_{sat} = \frac{m_n}{\phi_{open} \cdot V} \qquad \text{[eq.10]}$$

As previously stated, the thickness of the tablet will increase as liquid uptake occurs, which results in an increase in volume. Such increase will have an influence upon the porosity of the tablet. It is assumed that the density of the solid phase of the tablet is constant, and no mass is lost due to dissolution, leading to the volume of the solid phase remaining constant throughout. It can therefore be stated that the increase in volume will result in an increase in the porosity of the tablet. The volume of the solid phase is:

$$\frac{m_t}{\rho_s} = \left(1 - \phi_0\right) V_{tot,0} \qquad \text{[eq.11]}$$

where m_t is the initial mass of tablet (mass of solid phase), ρ_s is the density of the solid phase, and ϕ_0 and $V_{tot,0}$ are the porosity and volume of the tablet, respectively, prior to any liquid uptake. We can redefine this equation at any point in the experiment as a function of the tablet thickness bearing in mind its variation as the liquid uptake increases, as shown in Figure 6:

$$\frac{m_t}{\rho_s} = \left(1 - \phi\left(\delta\right)\right) V_{tot}\left(\delta\right) \qquad \text{[eq.12]}$$

Therefore it can be stated that:

$$\phi(\delta) = 1 - (1 - \phi_0)\frac{V_{tot,0}}{V_{tot}(\delta)} \quad \text{[eq.13]}$$

The total porosity will be the sum of the closed and open porosity of the tablet. It is assumed that the closed porosity remains constant throughout the experiment considering that the liquids selected cause no dissolution of the components; as such, the change in porosity will be solely due to change in open porosity:

$$\phi_{open}(\delta) = \phi_{tot} - \phi_{closed} = 1 - (1 - \phi_0)\frac{V_{tot,0}}{V_{tot}(\delta)} - (\phi_0 - \phi_{open,0}) \quad \text{[eq.14]}$$

Modeling the liquid uptake into the tablets

As described in Figure 4 and in previous works [21, 23], the liquid uptake from cycle to cycle can be measured by the difference in the force recorded by the tensiometer before dipping the solid in the pool of liquid and upon complete removal. The liquid uptake into the tablets for the experiments performed is represented in the map plotted in Figure 9, for which the properties of the liquids at experimental conditions are given in Table 2. This Figure presents a modified capillary number (*Ca*) that increases against the open porosity of the tablets. The *Ca* is defined as follows:

$$Ca = \frac{\mu}{\gamma} \cdot u^* \quad \text{[eq.15]}$$

where μ is the viscosity of the fluid, γ is the surface tension and u^* is a modified "velocity" of the liquid in the tablet corresponding to:

$$u^* = \frac{\Delta m^*}{\rho \cdot A} \quad \text{[eq.16]}$$

in which Δm^* is the rate of liquid uptake expressed as the ratio of the mass uptake that a tablet can hold (summarized in Table 1) at saturation to the time that such cycles lasts, which depends on the immersion rate of the solid into the liquid. In addition, ρ is the density of the liquid phase and A is the total surface area exposed to the liquid. This *Ca* plotted in the map takes into account the dipping speed of the experiment as well as the properties of the fluid (ρ, μ and γ), defined by the chemistry and the temperature at which the tests were performed, showing that the greater the porosity the higher the liquid penetration rate. The chemistry and the temperature at which tests were performed define the properties of the liquid, which are compiled in Table 2. One has to take into account the plot depicted in Figure 9 considers the values of the contact angle

of the liquid do not differ, which is a good approximation in this case considering the contact angles range from 80.57 ° to 85.87 °, which is an approximate difference of 6%.

Mathematical modelling can be utilized to test possible mechanisms involved in the liquid uptake during the experiments. Two models were produced taking into account the experimental information and the model for the contact area and volume throughout the process: the first will assume the liquid uptake is driven by a concentration gradient, the second that the uptake is driven by a pressure gradient.

Model 1: model based on uptake by mass gradient

The first model will assume that the uptake of liquid into the tablet is driven by the concentration difference between the concentration of liquid at any given time in the tablet and the saturation concentration, such that:

$$\left.\frac{\partial m_l}{\partial t}\right|_x = K \cdot A\big|_x \cdot \Delta C = K \cdot A\big|_x \cdot \left(C_{sat} - \frac{m_l\big|_x}{\phi_{open}(\delta).V\big|_x} \right) \qquad \text{[eq.17]}$$

The total mass of liquid in the tablet at any time will be the sum of all the masses at each discrete element in the tablet.

$$m_l(t) = \sum_{x=0}^{h_{\max}} m_l(t)\big|_x \qquad \text{[eq.18]}$$

K is the rate constant of the liquid flow into the porous tablet. This constant can be defined similarly to how Washburn's equation was constructed [30] for the penetration of liquids in pores, giving values of K of:

$$K = \frac{d_p \cdot \gamma \cdot \cos\theta}{4 \cdot \mu \cdot L_p} \qquad \text{[eq.19]}$$

where d_p is the weighted average pore diameter (as defined in equation 2), γ the surface tension, θ the contact angle between liquid and solid, μ the viscosity of the liquid. Note that this constant features the ratio of surface tension to viscosity, which can be envisaged as representative of speed of penetration of the liquid. Finally, L_p is a parameter that will be a function of the total pore length in the band taking into account factors related to the internal structure of the tablet, such as tortuosity, and will be estimated from the experimental data.

Model 2: model based on uptake by pressure gradient

This model assumes the transfer of liquid into the tablet will be pressure driven; thus, a model based on Darcy's law can be derived:

$$Q(t) = -\frac{\kappa \cdot A(t) \cdot \Delta P}{\mu \cdot L} \qquad \text{[eq.20]}$$

It was assumed that the length over which the pressure gradient acts is equal to half the tablet thickness. The difference in pressure ΔP at any point will be due to that of the hydrostatic pressure caused by the liquid above it and the capillary pressure, such that:

$$\Delta P = \rho_l \cdot g \cdot \left(h(t) - x\right) + \frac{2\gamma}{r_p}\cos\theta \qquad \text{[eq.21]}$$

Where γ is the surface tension of the liquid, r_p is the radius of the pores, assumed to be that of the capillaries and θ is the contact angle of the liquid with solid surface.

The flow rate, Q, can be defined as a change in mass:

$$Q = \frac{1}{\rho_l}\frac{\partial m_l}{\partial t} \qquad \text{[eq.22]}$$

Introducing these terms into Darcy's law gives:

$$\left.\frac{\partial m_l}{\partial t}\right| = \frac{\rho \cdot \kappa \cdot A|_x}{\mu \cdot L}\left(\rho_l \cdot g\left(h(t) - x\right) + \frac{2\gamma}{r_p}\cos\theta\right) \qquad \text{[eq.23]}$$

For each element the change in mass becomes

$$\left.\frac{\partial m_l}{\partial t}\right|_x = \frac{\rho \cdot \kappa \cdot A|_x}{\mu \cdot L}\left(\rho_l \cdot g \cdot \left(h(t) - x\right) + \frac{2\gamma}{r_p}\cos\theta\right) \qquad \text{[eq.24]}$$

Again, the total mass at any time is equal to the sum of the masses at each band, as described in equation 16 above.

The only unknown parameter in this model for this system is the permeability κ of the liquid into the tablet, which is dependent on the properties of the liquid and, therefore, temperature as well. In this model we must set the following constraint upon the mass, such that when the saturation concentration is reached there is no further liquid uptake, therefore:

$$\left.\frac{\partial m_l}{\partial t}\right|_x = 0, \qquad \text{for} \qquad m_l\big|_x \geq C_{sat}\cdot\phi_{open}(\delta)\cdot V\big|_x \qquad \text{[eq.25]}$$

Both for models 1 and 2, there is a requirement to define initial conditions. It will be assumed that the tablet has no liquid inside prior to the first cycle (c), therefore:

$$m_l\big|_{x,t,c} = 0, \qquad \forall x \in [0, h_{\max}], c = 1, t = 0 \qquad \text{[eq.26]}$$

The tablets will undergo a number of dipping cycles, and the initial conditions will be reset at the beginning of each cycle, where the new initial condition will be the mass of liquid in the tablet at the end of the previous cycle, such that:

$$m_l\big|_{x,t=0,c} = m_l\big|_{x,t=t_f,c-1}, \qquad \forall x \in [0, h_{\max}], \forall c, t \in (1, c_{tot}] \qquad \text{[eq.27]}$$

where, c_{tot} is the total number of cycles in each experiment.

Table 3 shows the optimized values for the parameters L_p and κ after fitting the two models described above to the experimental data. In addition, the mean squared errors (MSE) retrieved from the fittings and simulations are also included for the two models for each of the different experimental conditions. Additionally, Figure 10 shows the parity plot of the experimental results with respect to those predicted by the two models. Part (a) shows that Model 1 estimates the mass uptake values very well for all experiments after the first cycle, whilst Model 2 seems to underestimate slightly the uptake for the highest values, which corresponds to the tablets of highest porosities. On the other hand, both models seem to predict correct values of the liquid uptake at saturation of the tablets regardless of the mass increase value.

As the number of parameters being fitted in each model and the number of experimental data point used in the fitting were the same, the models can be compared directly from the mean squared error (MSE). For this reason, in statistical terms, the model based on mass gradient (Model 1) gives somewhat better results than that dealing with a pressure gradient (Model 2). Nevertheless, deeper discussion and understanding of the parameters obtained from these two must be made from a physical standpoint, for not only statistical considerations determine the validity or goodness of description of phenomena [45].

For Model 1, the values of the estimated parameter L_p were found to vary from a minimum value of 0.09 to a maximum of 5.12 m; they were mostly below 1 m. The values appear to be very large compared with what would be expected of the average

pore length within a tablet of such dimensions. However, an interpretation of this parameter is that it may combine pore length and tortuosity, with the value of the length being more in line with the expected total length of pores in the band.

Model 2 shows values of the permeability κ also with an order of magnitude of difference, with most values ranging between 0.03 and 0.51 D (1 D= 10^{-12} m^2). These values agree with common values estimated in previous studies for porous media of different nature. For instance, permeability values of up to 0.1 D for coal in sorptive reservoirs [46], 0.009 D for andesite rock [47], different glass beads bundles between 0.67 and 291.3 D [48] have been reported.

Furthermore, there appears to be a relationship whereby permeability increases as the open porosity and pore diameter increase. This can be observed in Figure 11 and has been described previously in literature [49].

For these reasons, despite the MSE being somewhat higher for Model 2, a more plausible physical explanation of the parameters suggests that a pressure driven model is a more credible representation of the involved phenomena in this study.

Simulation of the force balance

Taking into account the physical phenomena described in Figure 4, a model to describe the net force recorded by the tensiometer can be proposed, which slightly modifies that presented in previous works [23, 29]. This model will take into account the following forces:

- Weight of the liquid which is absorbed into the tablet (F_m)

$$F_m = g \cdot m_l \qquad \text{[eq.28]}$$

- Buoyancy of the tablet submerged in the liquid (F_B). The displaced volume will depend on the depth of the tablet, and the change in thickness of the tablet.

$$F_B = \rho_l \cdot g \cdot \int_0^{h(t)} \frac{R \cdot \delta \cdot \left(1+\cos\left(2\cos^{-1}\left(1-\frac{x}{R}\right)\right)\right)}{\sqrt{1-\left(1-\frac{x}{R}\right)^2}} dx \qquad \text{[eq.29]}$$

- Surface tension (F_γ), which acts on the wetted perimeter.

$$F_\gamma = 2\gamma\left(4R \cdot \sin\left(2 \cdot \cos^{-1}\left(1-\frac{h(t)}{R}\right)\right)+2\delta\right) \qquad \text{[eq.30]}$$

- Normal force due to flow of liquid (F_N).

$$F_N = \rho_l \cdot \delta \cdot R \cdot u^2 \qquad \text{[eq.31]}$$

- Drag force due to liquid flow around the tablet (F_D).

$$F_D = 2 \cdot \rho_l \cdot u^2 \cdot C_D \int_0^{h(t)} \frac{2R \cdot \left(1 - \cos\left(2 \cdot \cos^{-1}\left(1 - \frac{x}{R}\right)\right)\right)}{\sqrt{1 - \left(1 - \frac{x}{R}\right)^2}} dx \qquad \text{[eq.32]}$$

- Capillary force due to the flow of liquid into the pores of the tablet (F_{P_c})

$$F_{PC} = \frac{16 \cdot m_l \cdot \gamma}{\rho_l \cdot d_p^2} \cos\theta \qquad \text{[eq.33]}$$

The mass uptake (F_m) and surface tension forces (F_γ) will be positive and act towards the earth. On the other hand, buoyancy (F_m) and normal forces (F_N) will act in the opposite direction, hence taking a negative sign. Finally, the drag force (F_D) will depend upon the direction of flow: for the first half of the dipping it will be negative, yet when the liquid is being drained, the drag will be positive. The capillary force (F_{P_c}) will have both positive and negative components depending on whether the depth of the liquid is greater or lower than the radius of the tablet. Figure 12 shows a schematic of the direction of the forces. The main contributors to the force balance are the mass, buoyancy and surface tension, with the normal and drag forces having no significant influence upon the balance due to low liquid velocities. Therefore, allocating the corresponding signs, the net force acting on the tablet will result in:

$$F = F_m + F_\gamma - F_B - F_N \pm F_D \pm F_{PC} \qquad \text{[eq.34]}$$

In this case, no fitting was performed, but simulation of the balance following the two models described above was made. Comparing the force balances predicted by the two models, Model 1 shows a lower MSE value when compared to Model 2 (10.7 and 12.2, respectively, as seen in Table 3), although the difference between them is not as significant as with the mass balance.

Figure 12 depicts the evolution of the force measured throughout the first dipping cycle for four selected experiments, which are compared with the model as derived with the parameters obtained from Model 2, with more physical significance as discussed above. Considering that these experiments could well be performed using a precision balance, a model presenting the net force balance around the tablet can give an idea of the necessary precision to quantify such forces for a porous substrate of 0.25 g of mass. In addition, this experimental setup could have an application for measuring

the dissolution rate of porous bodies by monitoring the force balance around the solid substrate. It can be seen that for three of the plots in Figure 13, as occur for the majority of the experiments performed, the Model represents with good agreement the dynamic evolution of the force balance, although for the fourth plot presented for a tablet of 26.31%, the model appears to overestimate the net force. This is caused by an underestimation of the upward forces, predominantly buoyancy, in particular when the liquid is at the maximum depth (h_{max}). Also, there is a slight failure in the prediction of the time at which the breakage of the liquid bridge occurs (stage D in Figure 4), which according to the model takes place a few seconds earlier than observed.

Summary and Conclusions

This work deals with the preparation of porous substrates in the form of tablets and a subsequent coating process modeling both the process and the liquid uptake.

Particles of a relevant composition to the manufacture of powder detergent were compressed to generate porous substrates of variable porosities. As per X-ray microcomputed tomography measurements, the value of the overall porosity ranged from 54 % to 17 % when pressures from 0.75 to 15 MPa were tested and such porosity was found to follow a power law fit.

As a way to approach the coating of such substrates, dynamic wetting was proposed via a Wilhelmy plate technique consisting of dipping and withdrawal experiments in several cycles. The liquid uptake proved to be dependent mainly on the open porosity of the solid substrate and, to a lesser degree, the physicochemical properties of the liquids.

Two models were suggested to describe the mass uptake observed after subsequent cycles. Such models were based on the penetration driven by a mass gradient (Model 1) and a pressure gradient based on Darcy's law (Model 2) between the internal structure of the tablet and the bulk liquid. Despite the former showing a slightly better goodness of fit in statistical terms, the latter also fit well to the observed data and had more significance in physical terms. With this pressure driven model, the permeability of the solid medium was estimated to lie between 0.03 and 0.95 D and showed dependence on the open porosity and pore size.

Finally, the force balance was simulated with the results obtained from modelling the liquid uptake and compared against experimental observations. Whilst in

some cases the model represented with good agreement the observed evolution, in other cases the model overestimated the net force observed.

Acknowledgements

Funding of this project and fellowships for JE and TAHS were provided by the CHARIOT project (Grant number 31587-233189). CHARIOT is a three year project is partly funded by the government's Advanced Manufacturing Supply Chain Initiative (AMSCI) which aims to help existing UK supply chains grow and achieve World Class standards, while encouraging and retaining quality manufacturing in the UK.

We would also like to thank the Procter & Gamble company for supplying the materials for this work.

Abbreviations

Latin characters

A	area (m^2)
c	cycle
C	concentration ($kg\ m^{-3}$)
Ca	modified capillary number (non-dimensional)
C_D	drag coefficient (non-dimensional)
d	diameter (m)
D	darcy ($1\ D=10^{-12}\ m^2$)
g	gravity ($m\ s^{-2}$)
h	height of liquid relative to the bottom of the tablet (m)
K	rate constant of the liquid flow in to the porous tablet ($kg\ s^{-1}$)
L	length (m)
m	mass (kg)
MSE	mean squared error
P	pressure (MPa or $N\ m^{-2}$)
R	radius (m)
t	time (s)

u dipping speed (m s^{-1})

u* modified velocity of fluid penetrating into the substrate (m s^{-1})

V volume (m^3)

w weighting factor (-)

x distance above the tablet (m)

Greek characters

α angle formed between the center of the tablet and the liquid front (°)

δ thickness (m)

Δ increment

ϕ porosity (-)

γ surface tension (N m^{-1})

κ permeability (m^2)

μ viscosity (Pa s)

μ-CT X-ray microcomputed tomography

θ contact angle (°)

ρ density (kg m^{-3})

Subscripts

0 refers to initial state

B relative to buoyancy

D relative to drag

l refers to the liquid

m relative to mass

n relative to the cycle number

N normal

p refers to pore

P_C relative to capillary pressure

s refers to the solid

sat refers to saturated state

seg relative to circular segment

t refers to the tablet

References

(1) Gambaryan-Roisman, T. Liquids on porous layers: wetting, imbibition and transport processes. Current Opinion in Colloid & Interface Science **2014**, *19*, 320-335. doi: 10.1016/j.cocis.2014.09.001

(2) Klinzing, G. R.; Zavaliangos, A. A Simplified Model of Moisture Transport in Hydrophilic Porous Media With Applications to Pharmaceutical Tablets. J. Pharm. Sci. **2016**, *105*, 2410-2418. doi: 10.1016/j.xphs.2016.05.030

(3) Bawuah, P.; Chakraborty, M.; Ervasti, T.; Zeitler, J. A.; Ketolainen, J.; Gane, P. A. C.; Peiponen, K. E. A structure parameter for porous pharmaceutical tablets obtained with the aid of Wiener bounds for effective permittivity and terahertz time-delay measurement. Int. J. Pharm. **2016**, *506*, 87-92. doi: 10.1016/j.ijpharm.2016.04.026

(4) Yassin, S.; Goodwin, D. J.; Anderson, A.; Sibik, J.; Wilson, D. I.; Gladden, L. F.; Zeitler, J. A. The Disintegration Process in Microcrystalline Cellulose Based Tablets, Part 1: Influence of Temperature, Porosity and Superdisintegrants. J. Pharm. Sci. **2015**, *104*, 3440-3450. doi: 10.1002/jps.24544

(5) Kim, J. Y.; Kim, S. H.; Rhee, Y. S.; Park, C. W.; Park, E. S. Preparation of hydroxypropylmethyl cellulose-based porous matrix for gastroretentive delivery of gabapentin using the freeze-drying method. Cellulose **2013**, *20*, 3143-3154. doi: 10.1007/s10570-013-0048-7

(6) Bawuah, P.; Tan, N.; Tweneboah, S. N. A.; Ervasti, T.; Zeitler, J. A.; Ketolainen, J.; Peiponen, K. E. Terahertz study on porosity and mass fraction of active pharmaceutical

ingredient of pharmaceutical tablets. European Journal of Pharmaceutics and Biopharmaceutics **2016**, *105*, 122-133. doi: 10.1016/j.ejpb.2016.06.007

(7) Ervasti, T.; Silfsten, P.; Ketolainen, J.; Peiponen, K. E. A Study on the Resolution of a Terahertz Spectrometer for the Assessment of the Porosity of Pharmaceutical Tablets. Appl. Spectrosc. **2012**, *66*, 319-323. doi: 10.1366/11-06315

(8) Manickam, S. S.; Gelb, J.; McCutcheon, J. R. Pore structure characterization of asymmetric membranes: Non-destructive characterization of porosity and tortuosity. Journal of Membrane Science **2014**, *454*, 549-554. doi: 10.1016/j.memsci.2013.11.044

(9) Betz, O.; Wegst, U.; Weide, D.; Heethoff, M.; Helfen, L.; Lee, W. K.; Cloetens, P. Imaging applications of synchrotron X-ray phase-contrast microtomography in biological morphology and biomaterials science. 1. General aspects of the technique and its advantages in the analysis of millimetre-sized arthropod structure. Journal of Microscopy-Oxford **2007**, *227*, 51-71. doi: 10.1111/j.1365-2818.2007.01785.x

(10) Okochi, T. A nondestructive dendrochronological study on japanese wooden shinto art sculptures using micro-focus X-ray Computed Tomography (CT) Reviewing two methods for scanning objects of different sizes. Dendrochronologia **2016**, *38*, 1-10. doi: 10.1016/j.dendro.2016.01.004

(11) Schoeman, L.; Williams, P.; du Plessis, A.; Manley, M. X-ray micro-computed tomography (mu CT) for non-destructive characterisation of food microstructure. Trends in Food Science & Technology **2016**, *47*, 10-24. doi: 10.1016/j.tifs.2015.10.016

(12) Alghunaim, A.; Kirdponpattara, S.; Newby, B. M. Z. Techniques for determining contact angle and wettability of powders. Powder Technol. **2016**, *287*, 201-215. doi: 10.1016/j.powtec.2015.10.002

(13) Hapgood, K. P.; Litster, J. D.; Biggs, S. R.; Howes, T. Drop penetration into porous powder beds. J. Colloid Interface Sci. **2002**, *253*, 353-366. doi: 10.1006/jcis.2002.8527

(14) Nguyen, T.; Shen, W.; Hapgood, K. Drop penetration time in heterogeneous powder beds. Chem. Eng. Sci. **2009**, *64*, 5210-5221. doi: 10.1016/j.ces.2009.08.038

(15) Nowak, E.; Robbins, P.; Combes, G.; Stitt, E. H.; Pacek, A. W. Measurements of contact angle between fine, non-porous particles with varying hydrophobicity and water and non-polar liquids of different viscosities. Powder Technol. **2013**, *250*, 21-32. doi: 10.1016/j.powtec.2013.09.001

(16) Starov, V. M.; Zhdanov, S. A.; Kosvintsev, S. R.; Sobolev, V. D.; Velarde, M. G. Spreading of liquid drops over porous substrates. Adv. Colloid Interface Sci. **2003**, *104*, 123-158. doi: 10.1016/s0001-8686(03)00039-3

(17) Lazghab, M.; Saleh, K.; Pezron, I.; Guigon, P.; Komunjer, L. Wettability assessment of finely divided solids. Powder Technol. **2005**, *157*, 79-91. doi: 10.1016/j.powtec.2005.05.014

(18) Trabi, C. L.; Ouali, F. F.; McHale, G.; Javed, H.; Morris, R. H.; Newton, M. I. Capillary Penetration into Inclined Circular Glass Tubes. Langmuir **2016**, *32*, 1289-1298. doi: 10.1021/acs.langmuir.5b03904

(19) Subrahmanyam, T. V.; Prestidge, C. A.; Ralston, J. Contact angle and surface analysis studies of sphalerite particles. Miner. Eng. **1996**, *9*, 727-741. doi: 10.1016/0892-6875(96)00064-7

(20) Prestidge, C. A.; Ralston, J. Contact angle studies of galena particles. J. Colloid Interface Sci. **1995**, *172*, 302-310. doi: 10.1006/jcis.1995.1256

(21) Moghaddam, M. S.; Claesson, P. M.; Walinder, M. E. P.; Swerin, A. Wettability and liquid sorption of wood investigated by Wilhelmy plate method. Wood Science and Technology **2014**, *48*, 161-176. doi: 10.1007/s00226-013-0592-1

(22) Moghaddam, M. S.; Heydari, G.; Tuominen, M.; Fielden, M.; Haapanen, J.; Makela, J. M.; Walinder, M. E. P.; Claesson, P. M.; Swerin, A. Hydrophobisation of wood surfaces by combining liquid flame spray (LFS) and plasma treatment: dynamic wetting properties. Holzforschung **2016**, *70*, 527-537. doi: 10.1515/hf-2015-0148

(23) Moghaddam, M. S.; Walinder, M. E. P.; Claesson, P. M.; Swerin, A. Multicycle Wilhelmy Plate Method for Wetting Properties, Swelling and Liquid Sorption of Wood. Langmuir **2013**, *29*, 12145-12153. doi: 10.1021/la402605q

(24) Moghaddam, M. S.; Walinder, M. E. P.; Claesson, P. M.; Swerin, A. Wettability and swelling of acetylated and furfurylated wood analyzed by multicycle Wilhelmy plate method. Holzforschung **2016**, *70*, 69-77. doi: 10.1515/hf-2014-0196

(25) Son, J.; Gardner, D. J. Dimensional stability measurements of thin wood veneers using the Wilhelmy plate technique. Wood and Fiber Science **2004**, *36*, 98-106. doi:

(26) Buckton, G. Assessment of the wettability of pharmaceutical powders. J. Adhes. Sci. Technol. **1993**, *7*, 205-219. doi: 10.1163/156856193x00664

(27) Chawla, A.; Buckton, G.; Taylor, K. M. G.; Newton, J. M.; Johnson, M. C. R. Wilhelmy plate contact-angle data on powder compacts - considerations of plate perimeter. European Journal of Pharmaceutical Sciences **1994**, *2*, 253-258. doi: 10.1016/0928-0987(94)90030-2

(28) Pepin, X.; Blanchon, S.; Couarraze, G. A new approach for determination of powder wettability. Int. J. Pharm. **1997**, *152*, 1-5. doi: 10.1016/s0378-5173(97)04868-0

(29) Tretinnikov, O. N.; Ikada, Y. Dynamic wetting and contact-angle hysteresis of polymer surfaces studies with the modified Wilhelmy balance method. Langmuir **1994**, *10*, 1606-1614. doi: 10.1021/la00017a047

(30) Washburn, E. W. The Dynamics of Capillary Flow. Physical Review **1921**, *17*, 273. doi:

(31) Liu, G. D.; Zhang, M. Y.; Ridgway, C.; Gane, P. Spontaneous Inertial Imbibition in Porous Media Using a Fractal Representation of Pore Wall Rugosity. Transport in Porous Media **2014**, *104*, 231-251. doi: 10.1007/s11242-014-0331-6

(32) Schoelkopf, J.; Gane, P. A. C.; Ridgway, C. J.; Matthews, G. P. Practical observation of deviation from Lucas-Washburn scaling in porous media. Colloids and Surfaces a-Physicochemical and Engineering Aspects **2002**, *206*, 445-454. doi: 10.1016/s0927-7757(02)00066-3

(33) Liu, G. D.; Zhang, M. Y.; Ridgway, C.; Gane, P. Pore wall rugosity: The role of extended wetting contact line length during spontaneous liquid imbibition in porous media. Colloids and Surfaces a-Physicochemical and Engineering Aspects **2014**, *443*, 286-295. doi: 10.1016/j.colsurfa.2013.11.033

(34) Cai, J. C.; Hu, X. Y.; Standnes, D. C.; You, L. J. An analytical model for spontaneous imbibition in fractal porous media including gravity. Colloids and Surfaces a-Physicochemical and Engineering Aspects **2012**, *414*, 228-233. doi: 10.1016/j.colsurfa.2012.08.047

(35) Ding, X. Y.; Ebin, J. P.; Harris, T. A. L.; Li, Z.; Fuller, T. F. Analytical Models for Predicting Penetration Depth During Slot Die Coating onto Porous Media. AlChE J. **2014**, *60*, 4241-4252. doi: 10.1002/aic.14570

(36) Ding, X. Y.; Fuller, T. F.; Harris, T. A. L. A simulation model to approximate penetration of a non-Newtonian fluid into a porous media during slot die coating.

Journal of Coatings Technology and Research **2014**, *11*, 83-87. doi: 10.1007/s11998-013-9501-7

(37) Esteban, J.; Murasiewicz, H.; Simons, T. A. H.; Bakalis, S.; Fryer, P. J. Measuring the Density, Viscosity, Surface Tension, and Refractive Index of Binary Mixtures of Cetane with Solketal, a Novel Fuel Additive. Energy & Fuels **2016**, *30*, 7452-7459. doi: 10.1021/acs.energyfuels.6b01992

(38) Kawakita, K.; Ludde, K. H. Some considerations on powder compression equations. Powder Technol. **1971**, *4*, 61-68. doi: 10.1016/0032-5910(71)80001-3

(39) Denny, P. J. Compaction equations: a comparison of the Heckel and Kawakita equations. Powder Technol. **2002**, *127*, 162-172. doi: 10.1016/s0032-5910(02)00111-0

(40) Brielles, N.; Chantraine, F.; Viana, M.; Chulia, D.; Branlard, P.; Rubinstenn, G.; Lequex, F.; Lasseux, D.; Birot, M.; Roux, D.; Mondain-Monval, O. Imbibition and dissolution of a porous medium. Industrial & Engineering Chemistry Research **2007**, *46*, 5785-5793. doi: 10.1021/ie0701569

(41) Zhang, Y. H.; Xu, X. M.; Lebedev, M.; Sarmadivaleh, M.; Barifcani, A.; Iglauer, S. Multi-scale x-ray computed tomography analysis of coal microstructure and permeability changes as a function of effective stress. International Journal of Coal Geology **2016**, *165*, 149-156. doi: 10.1016/j.coal.2016.08.016

(42) Qsymah, A.; Sharma, R.; Yang, Z.; Margetts, L.; Mummery, P. Micro X-ray computed tomography image-based two-scale homogenisation of ultra high performance fibre reinforced concrete. Construction and Building Materials **2017**, *130*, 230-240. doi: 10.1016/j.conbuildmat.2016.09.020

(43) Schock, J.; Liebl, S.; Achterhold, K.; Pfeiffer, F. Obtaining the spacing factor of microporous concrete using high-resolution Dual Energy X-ray Micro CT. Cem. Concr. Res. **2016**, *89*, 200-205. doi: 10.1016/j.cemconres.2016.08.008

(44) Yang, B. H.; Wu, A. X.; Miao, X. X.; Liu, J. Z. 3D characterization and analysis of pore structure of packed ore particle beds based on computed tomography images. Transactions of Nonferrous Metals Society of China **2014**, *24*, 833-838. doi: 10.1016/s1003-6326(14)63131-9

(45) Esteban, J.; Fuente, E.; Blanco, A.; Ladero, M.; Garcia-Ochoa, F. Phenomenological kinetic model of the synthesis of glycerol carbonate assisted by focused beam reflectance measurements. Chem. Eng. J. **2015**, *260*, 434-443. doi: 10.1016/j.cej.2014.09.039

(46) Feng, R.; Liu, J.; Harpalani, S. Optimized pressure pulse-decay method for laboratory estimation of gas permeability of sorptive reservoirs: Part 1-Background and numerical analysis. Fuel **2017**, *191*, 555-564. doi: 10.1016/j.fuel.2016.11.079

(47) Cid, H. E.; Carrasco-Nunez, G.; Manea, V. C. Improved method for effective rock microporosity estimation using X-ray microtomography. Micron (Oxford, England : 1993) **2017**, *97*, 11-21. doi: 10.1016/j.micron.2017.01.003

(48) Jiang, L.; Liu, Y.; Teng, Y.; Zhao, J.; Zhang, Y.; Yang, M.; Song, Y. Permeability estimation of porous media by using an improved capillary bundle model based on micro-CT derived pore geometries. Heat Mass Transfer. **2017**, *53*, 49-58. doi: 10.1007/s00231-016-1795-4

(49) Bhattacharya, A.; Calmidi, V. V.; Mahajan, R. L. Thermophysical properties of high porosity metal foams. Int. J. Heat Mass Transfer **2002**, *45*, 1017-1031. doi: 10.1016/s0017-9310(01)00220-4

Figure captions

Figure 1. (a) Schematic representation of the experimental setup. (b) Detail of the tablet dipping into the liquid reservoir

Figure 2. 3D reconstruction of μ-CT scans of tablets compressed at (a) 0.75 MPa and (b) 15 MPa at a rate of 0.5 mm s^{-1}.

Figure 3. Porosity of the substrates applying different forming pressures. Data points and error bars correspond to the average and standard deviations of replicate experiments. Solid line represents the power law fit to the data as defined by equation 1.

Figure 4. Description of the dynamics of an experiment: dipping a cylindrical porous substrate into a liquid pool (inspired by [23]). Conditions: tablet of 25.76 % porosity, liquid at 40 C and immersion rate of 10 mm min^{-1}.

Figure 5. Images of tablets taken under a fluorescent microscope after performing different wetting experiments in Neodol 45-7 at 40 C: (a) tablet of porosity 43.55% after 6 consecutive immersion cycles and (b) tablet of porosity 18.99% after 1 immersion cycle.

Figure 6. Variation of the thickness of the tablet with respect to the change of mass observed

Figure 7. Schematic representation of the integration of the bands of the immersed tablet into the liquid

Figure 8. Observed and modelled mass uptake as a function of the contact cycles in the dipping experiments for selected experiments.

Figure 9. Plot of the modified capillary number obtained for each experiment against the open porosity available for liquid uptake.

Figure 10. Relationship between the estimated permeability and the open porosity and pore size as measured by μ-CT.

Figure 11. Scheme of the direction of the forces taking place in the dipping experiment. Solid and dashed lines represent major and minor contributors to the net force, respectively.

Figure 12. Dynamics of the net force observed the experiment and model prediction in selected experiments performed in tablets of different porosities.

Table captions

Table 1. Weighted average of the pore size based on the pore size distribution on the powder preparations as measured by X-ray microcomputed tomography

Table 2. Density, viscosity and surface tension of the liquids tested at different temperatures.

Table 3. Estimated values of the parameters for and mean squared errors obtained from the simulation of the experiments

Figure 1. (a) Schematic representation of the experimental setup. (b) Detail of the tablet dipping into the liquid reservoir. List of elements: 1. Computer for data acquisition; 2. Temperature controlled water bath; 3. Syringe pump; 4. Tensiometer balance; 5. Porous solid sample; 6. Liquid reservoir within a vessel; 7. Jacket for temperature conditioning.

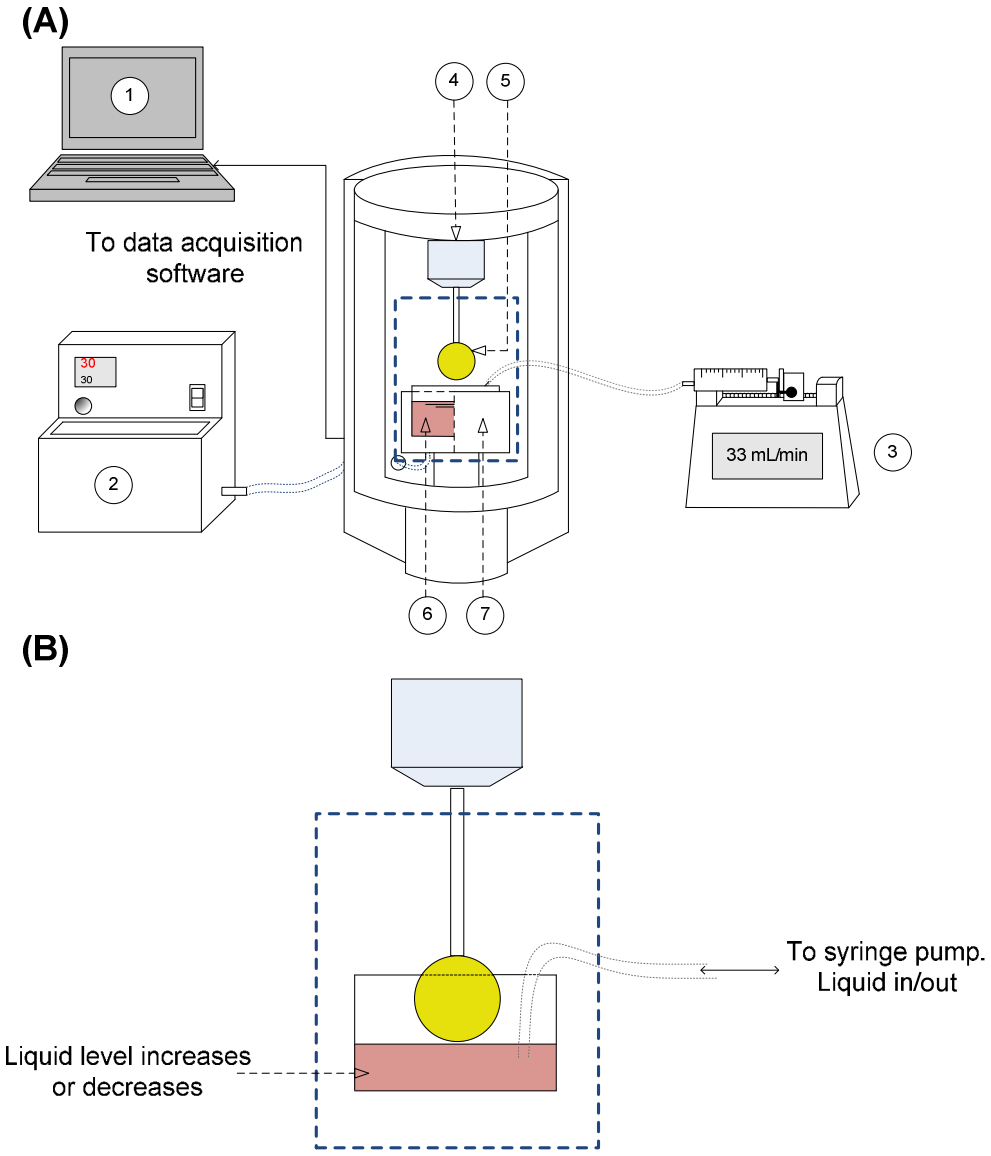

Figure 2. 3D reconstruction of μ-CT scans of tablets compressed at (a) 0.75 MPa and (b) 15 MPa showing the difference in thickness and porosity.

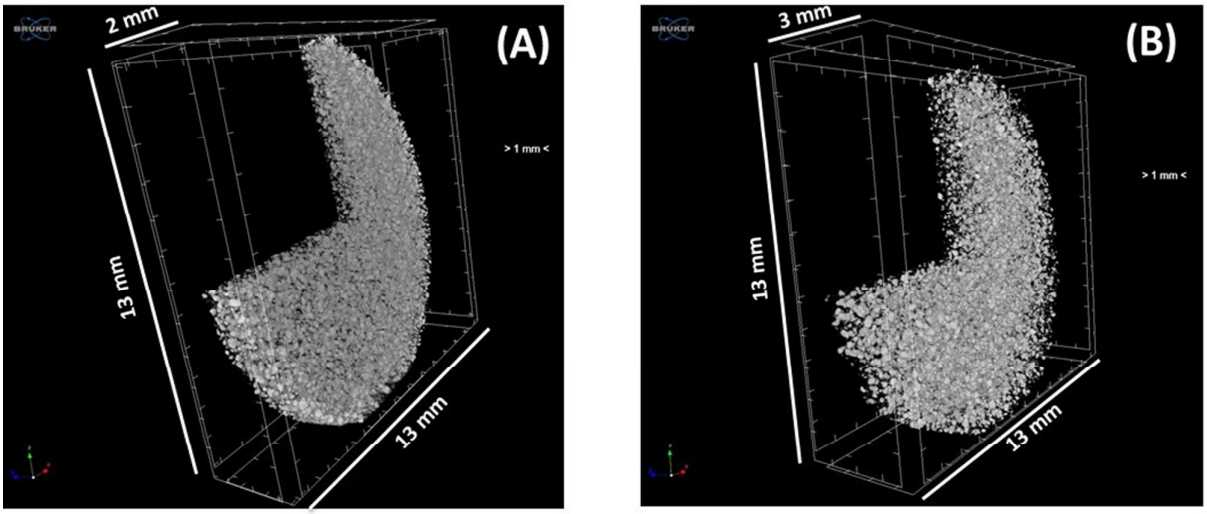

Figure 3. Porosity of the substrates applying different pressures. Data correspond to the average of three replicate experiments. The solid line represents the fit of the Kawakita equation to the data as defined by equation (1).

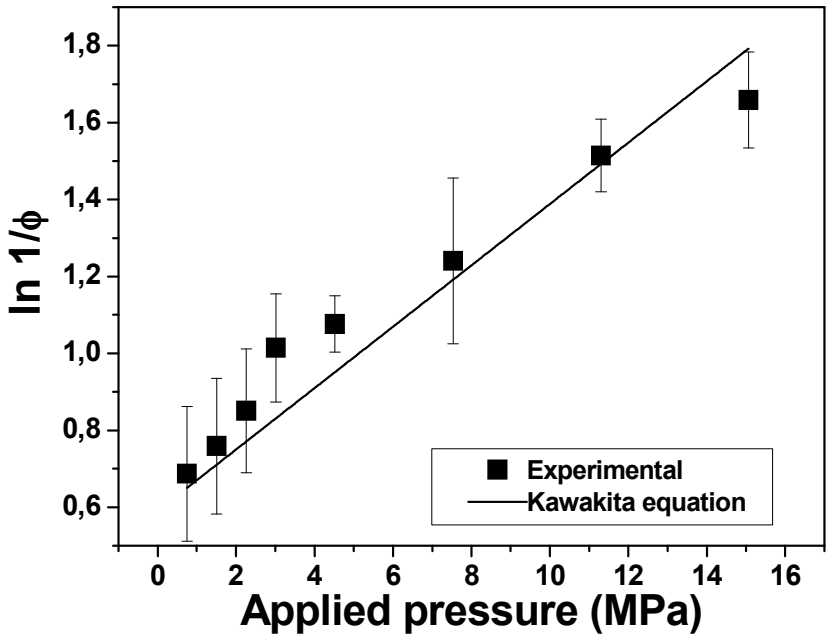

Figure 4. Description of an experiment: dipping a tablet into a liquid pool. Conditions: tablet of 25.76 % porosity, liquid at 40 C and immersion rate of 10 mm min^{-1}.

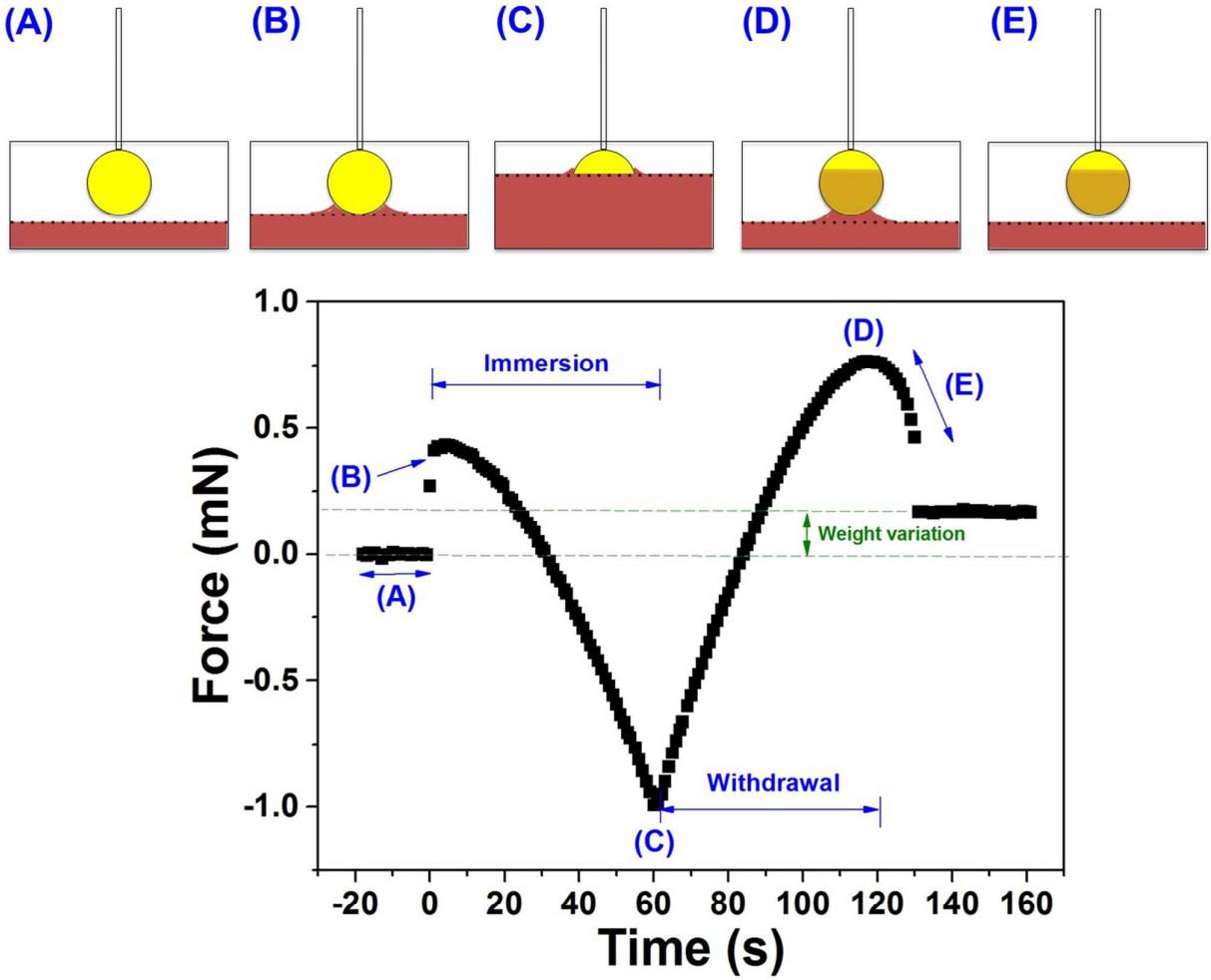

Figure 5. Images of tablets taken under a fluorescent microscope after different wetting experiments in Neodol 45-7 at 40 C: (a) tablet of porosity 43.55% after 6 consecutive immersion cycles and (b) tablet of porosity 18.99% after 1 immersion cycle.

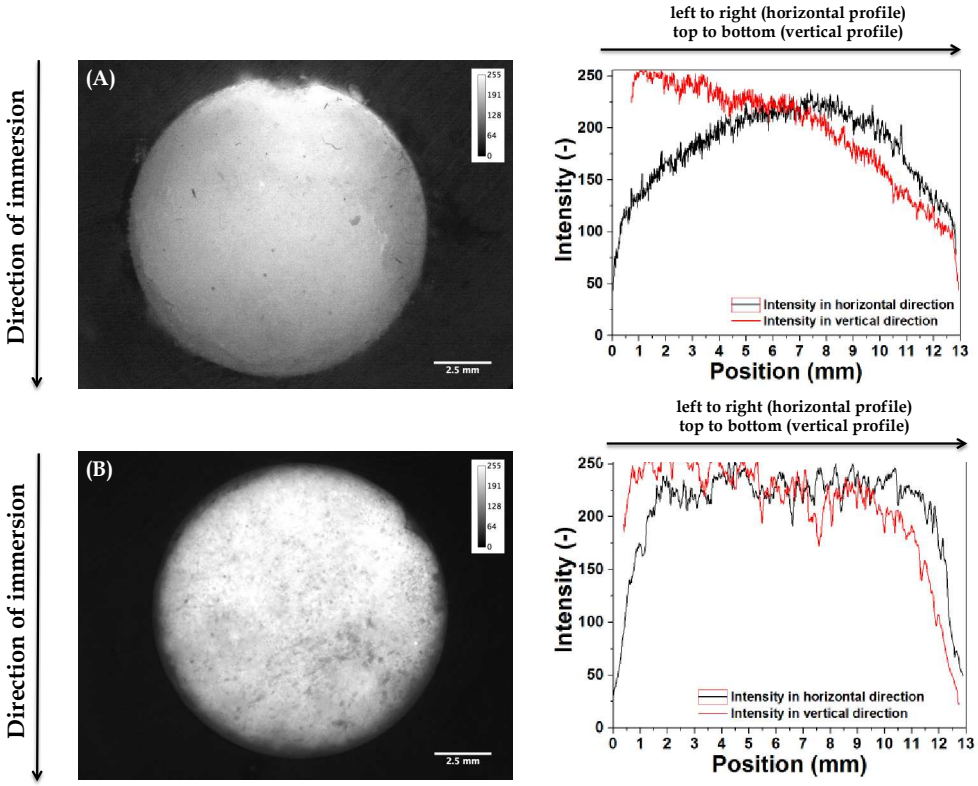

Figure 6. Variation of the thickness of the tablet with respect to the change of mass observed

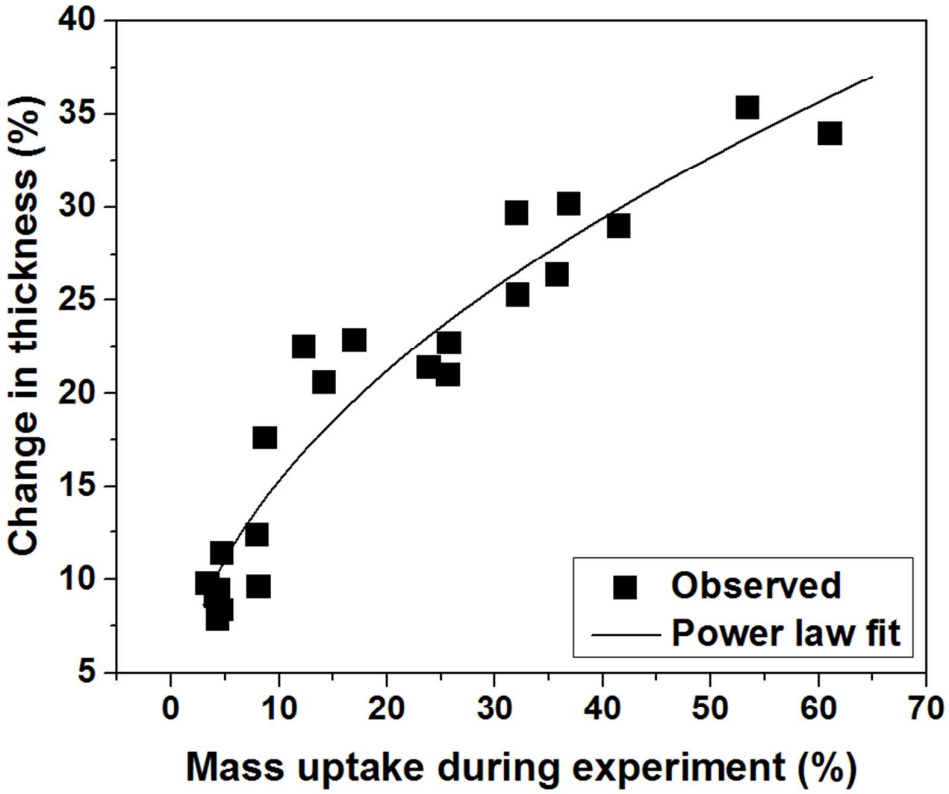

Figure 7. Schematic representation of the integration of the bands and angle of the immersed tablet into the liquid

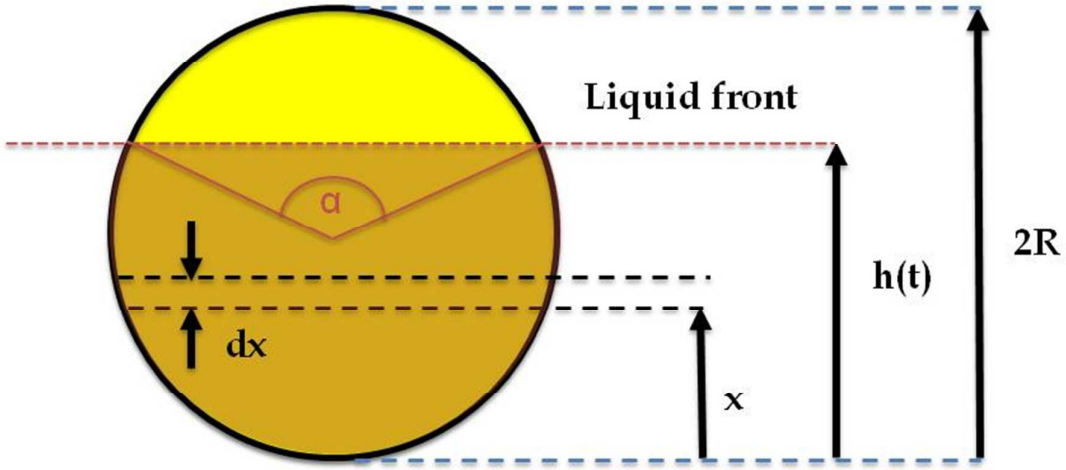

Figure 8. Observed and modelled mass uptake as a function of the contact cycles in the dipping experiments for selected experiments.

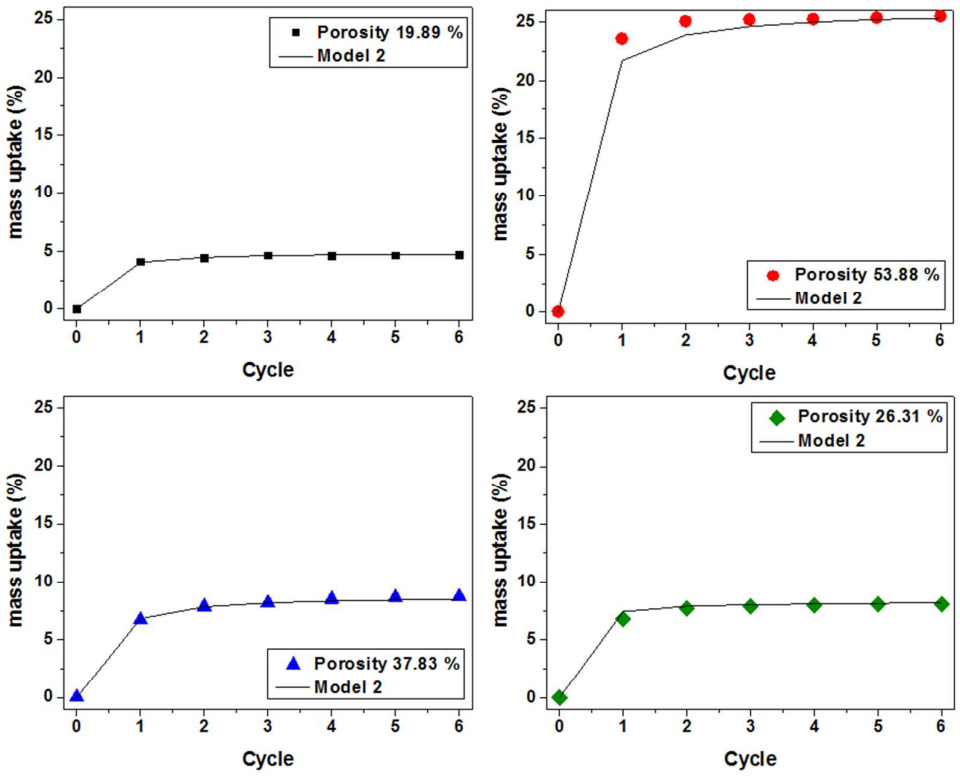

Figure 9. Plot of the modified capillary number obtained for each experiment against the open porosity available for liquid uptake.

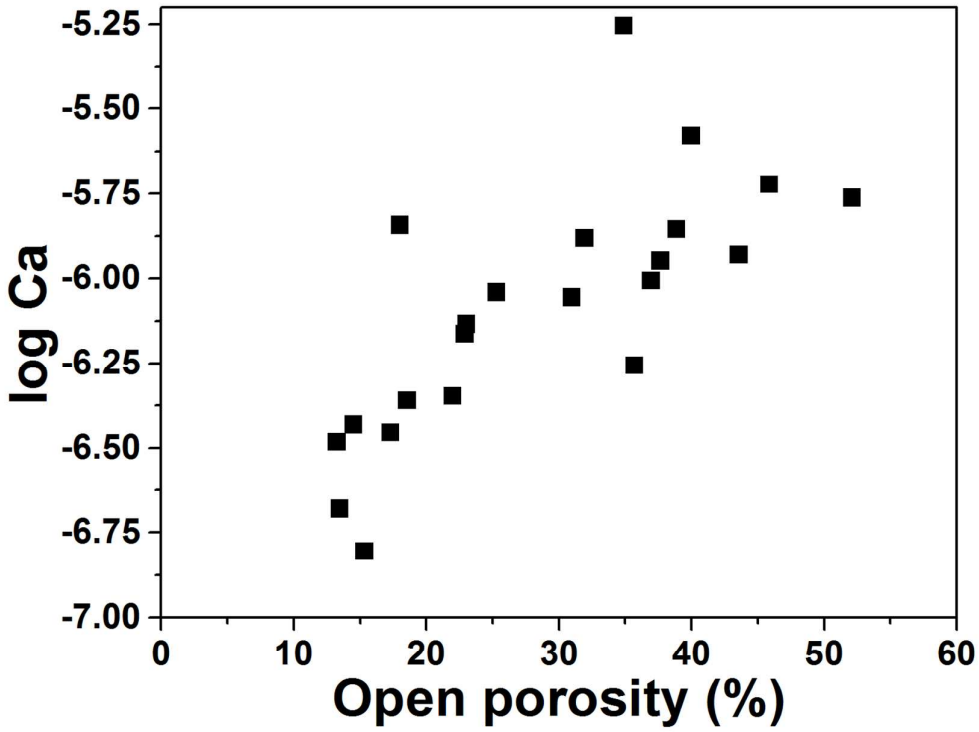

Figure 10. Parity plot of the observed values for the mass uptake in tablets for all the experiments performed (a) after the first immersion cycle and (b) at saturation of the tablet

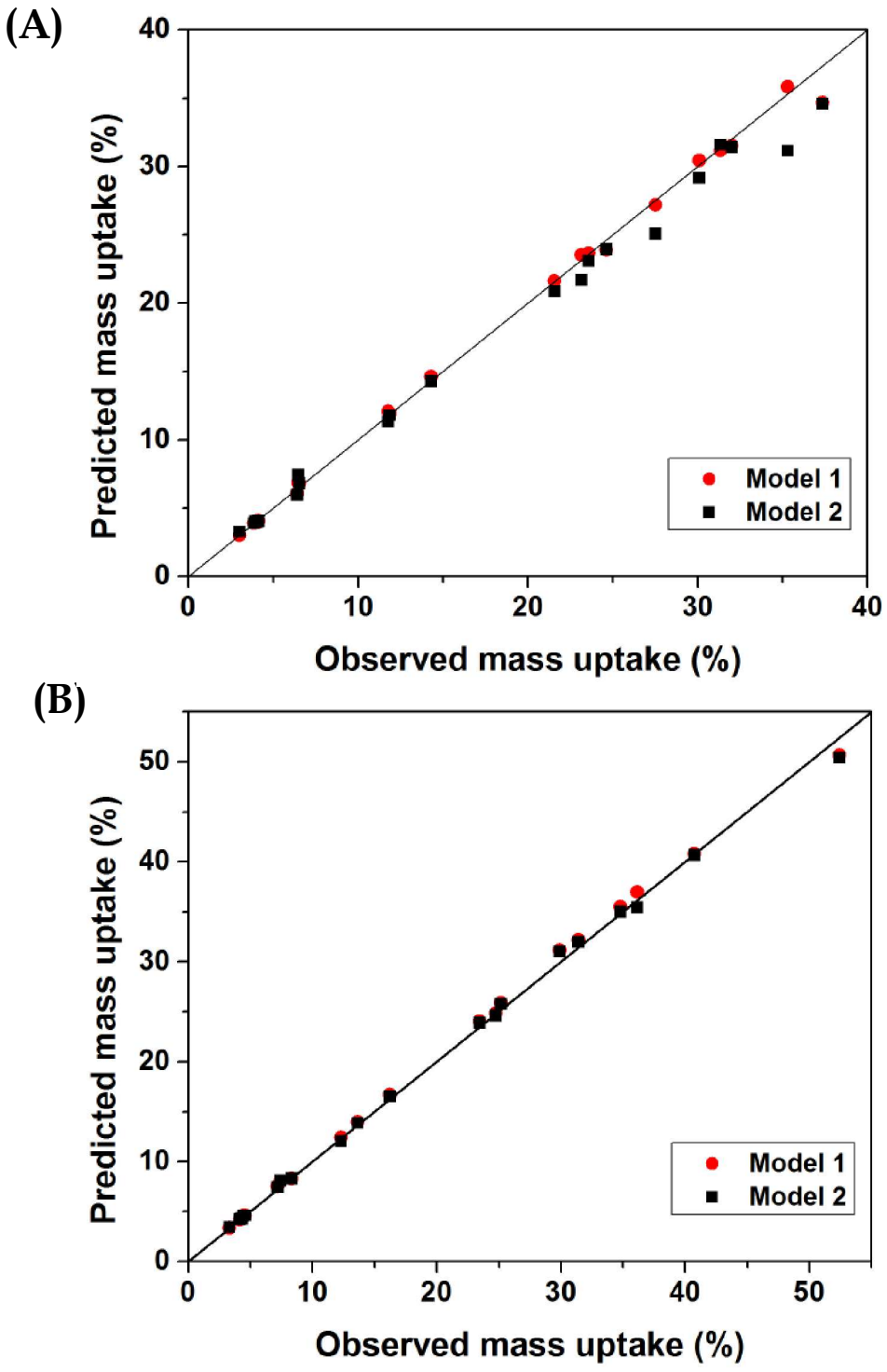

Figure 11. Relationship between the estimated permeability and the open porosity and pore size as measured by μ-CT. (a) Surface plot and (b) surface projection.

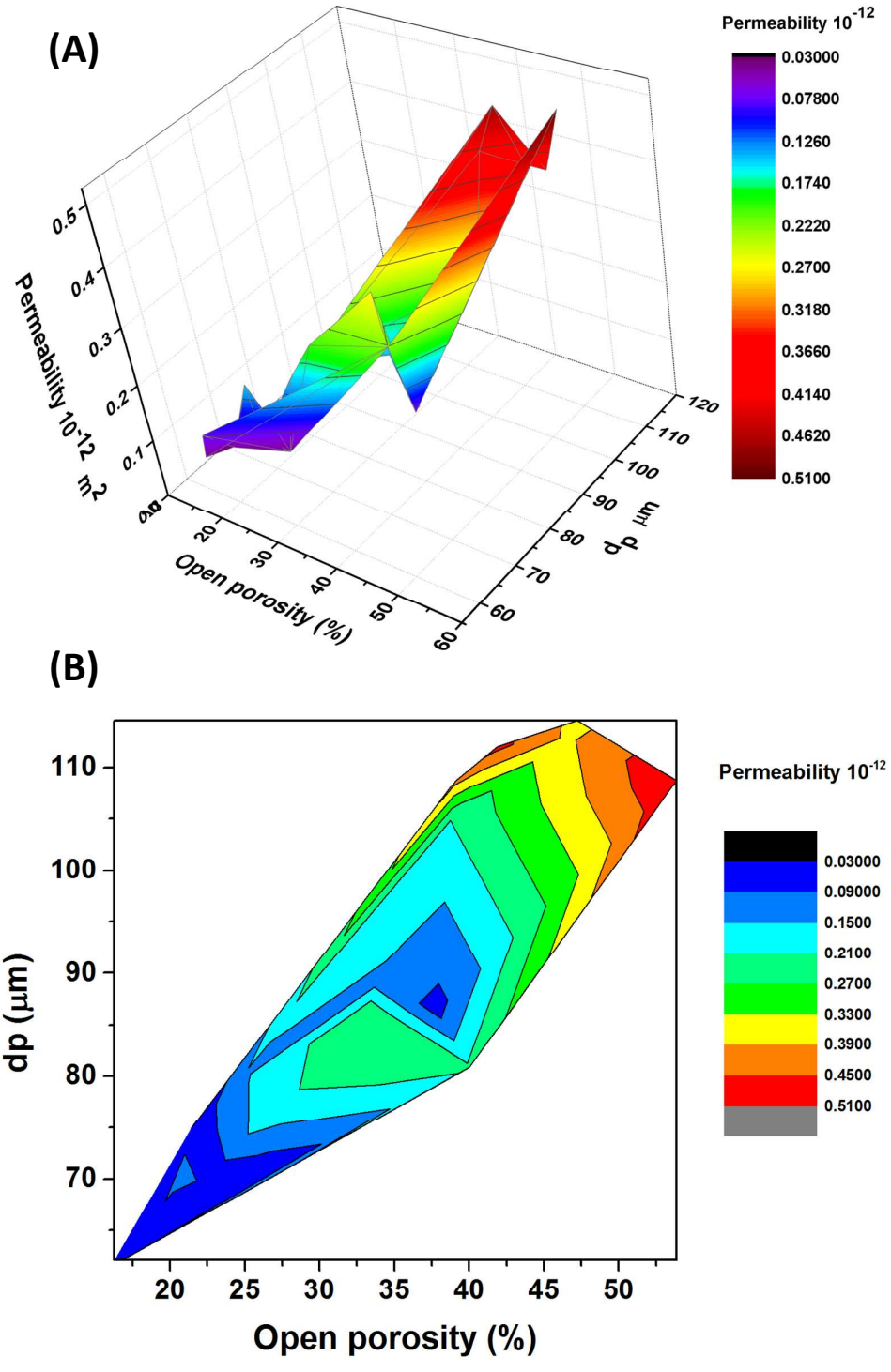

Figure 12. Scheme of the direction of the forces taking place in the dipping experiment. Solid and dashed lines represent major and minor contributors to the net force, respectively.

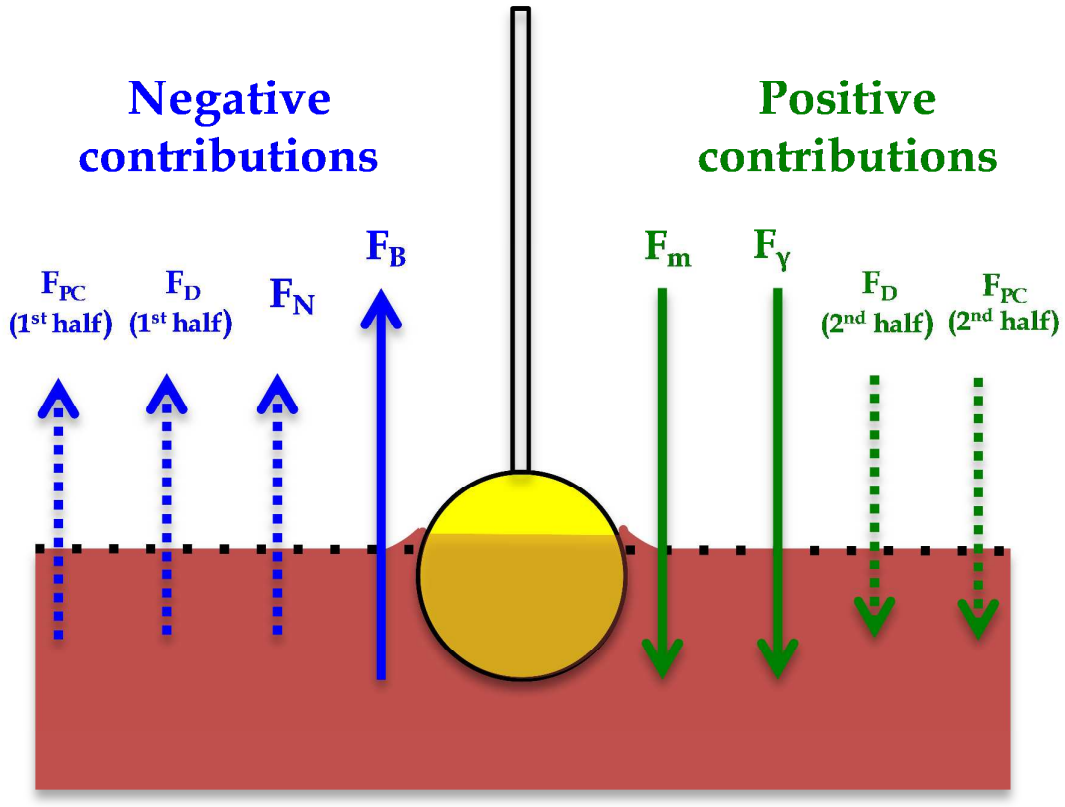

Figure 13. Dynamics of the net force observed the experiment and model prediction in selected experiments performed in tablets of different porosities.

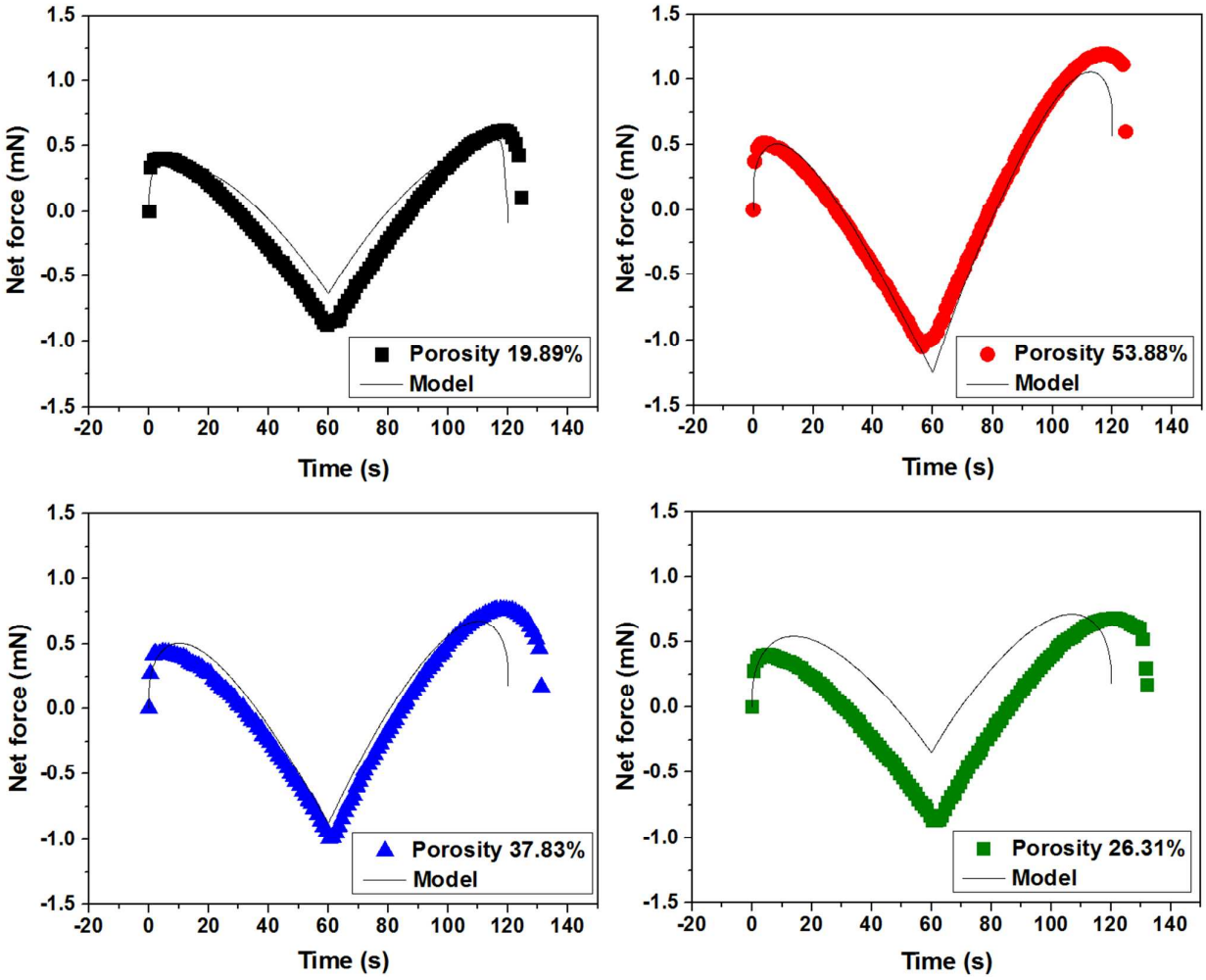

Table 1. Experimental conditions and porosity of the tablets used and final mass uptake.

Run	Liquid used	Temperature (C)	Applied normal stress (MPa)	Overall porosity (%)	Open porosity (%)	d_p (μm)	Mass uptake at saturation (%)
1	Neodol 45-7	40	2000	19.89	14.47	68.11	4.59
2	Neodol 45-7	40	100	53.88	52.1	108.75	24.76
3	Neodol 45-7	40	400	37.83	35.7	86.37	8.30
4	Neodol 45-7	30	2000	26.31	23.01	70.53	7.40
5	Neodol 45-7	30	2000	21.41	17.3	74.93	3.30
6	Neodol 45-7	30	2000	22.66	18.54	70.12	4.22
7	Neodol 45-7	50	400	47.23	45.84	114.53	36.14
8	Neodol 45-7	60	2000	46.55	43.55	112.94	31.41
9	Neodol 45-7	50	400	33.21	31.91	85.98	25.17
10	Neodol 45-7	60	200	33.69	30.95	88.87	23.44
11	Neodol 45-7 + oleic acid (50:50 w/w)	30	200	37.43	34.87	91.99	34.78
12	Neodol 45-7 + oleic acid (50:50 w/w)	30	400	20.44	18.01	69.39	7.17
13	Neodol 45-7 + oleic acid (50:50 w/w)	30	400	40.02	36.93	80.85	29.90
14	Oleic acid	25	200	41.88	39.95	112.03	59.90
15	Oleic acid	40	200	39.11	38.85	108.75	40.73
16	Oleic acid	50	200	38.74	37.66	104.85	52.41
17	Oleic acid	25	600	27.88	25.26	77.5	13.62
18	Oleic acid	40	600	25.23	22.88	74.38	16.22
19	Oleic acid	50	600	24.71	21.94	79.72	12.29
20	Oleic acid	25	2000	16.27	13.22	62.12	4.42
21	Oleic acid	40	2000	17.04	13.44	62.32	4.14
22	Oleic acid	50	2000	19.04	15.32	66.65	4.31

Table 2. Physical properties of the liquids employed for the coating experiments.

Liquid	Contact angle[a] (°)	Temperature (C)	Viscosity (mPa s)	Density (kg m^{-3})	Surface tension (mN m^{-1})
Neodol 45-7	80.57 ± 2.73	30	46.77	977.5	32.49
Neodol 45-7		40	36.75	969.0	31.97
Neodol 45-7		50	24.31	962.6	31.48
Neodol 45-7		60	17.24	955.2	30.94
Neodol 45-7 + oleic acid (50:50 w/w)	85.02 ± 1.29	30	35.04	933.3	32.10
Oleic acid	85.87 ± 5.87	25	30.47	890.4	32.56
Oleic acid		30	25.34	887.7	32.20
Oleic acid		40	18.46	880.1	31.75
Oleic acid		50	13.89	873.3	30.43

[a] Measured using a DSA 30S Drop Size Analyser (Krüss, Hamburg, Germany). Measurements at room temperature.

Table 3. Estimated values of the parameters for the two models and mean squared errors obtained from the simulation of the experiments

	Model 1			Model 2		
Experiment Number	L_p**(m)**	**MSE liquid uptake**	**MSE Net force**	$\kappa \bullet 10^{12}$ **(m^2)**	**MSE liquid uptake**	**MSE Net force**
1	0.54	0.005	0.254	0.03	0.004	0.288
2	0.09	0.023	0.245	0.51	0.494	0.266
3	0.29	0.016	0.243	0.07	0.017	0.260
4	0.70	0.003	0.347	0.04	0.070	0.366
5	0.60	0.003	0.292	0.04	0.016	0.314
6	0.23	0.000	0.184	0.05	0.000	0.219
7	0.08	0.020	0.810	0.37	7.479	0.819
8	0.17	0.035	0.726	0.38	0.419	0.791
9	0.21	0.080	0.536	0.27	0.155	0.609
10	0.35	0.076	0.549	0.14	0.205	0.603
11	0.44	0.233	0.513	0.95	1.060	0.668
12	0.91	0.115	0.184	0.15	0.108	0.191
13	2.14	0.413	0.165	0.22	0.316	0.244
14	2.51	3.981	1.164	0.47	4.258	1.359
15	2.10	0.399	1.063	0.41	0.348	1.298
16	5.12	2.819	0.919	0.21	3.394	1.150
17	1.22	0.008	0.573	0.20	0.011	0.658
18	2.00	0.028	0.682	0.15	0.053	0.737
19	0.83	0.038	0.381	0.14	0.155	0.464
20	2.44	0.009	0.173	0.04	0.008	0.179
21	1.24	0.016	0.380	0.08	0.017	0.404
22	2.66	0.003	0.328	0.04	0.003	0.352
	Total MSE	8.323	10.711	Total MSE	18.590	12.239

For table of contents use only